TECHNISCHE UNIVERSITÄT MÜNCHEN
LEHRSTUHL A FÜR THERMODYNAMIK
o. PROF. DR.-ING. F. MAYINGER

Heat Transfer and Void Fraction of Dispersed Two-Phase Flow in 90° Circular Bends

Paper E 1

by

M.J. Wang, F. Mayinger

presented at

European Two-Phase Flow Group Meeting
Varese (Italy), May 21 - 23, 1990

Heat Transfer and Void Fraction of Dispersed Two-Phase Flow in 90^0 Circular Bends

M.J. Wang F. Mayinger

Lehrstuhl A für Thermodynamik
Technische Universität München

Abstract

This paper presents measurements of void-fraction and heat transfer of dispersed droplet flow in 90^0 circular bends with the refrigerant R12 as modeling fluid. The experiments were carried out at various mass fluxes 400 - 2000 kg/m^{2}s, critical pressure ratios 0.23 - 0.7, wall heat fluxes 20 - 70 kw/m^2, inlet equilibrium qualities 0.45 - 1.15 and mean radius ratios of bend to tube 28 and 42. Local void distributions were measured by an impedance-void-meter over the five different regions of cross-section and at different bend angular positions (15^0, 30^0, 60^0 for R = 400 mm; 45^0, 90^0 for R = 600 mm)

As shown by the void fraction measurements, droplet distribution exhibits a distinct non-symmetric character with the maximum concentration skewed to the outer wall region of the bend. Serious phase separation occurs early in the downstream of bend inlet and then develops until about 60^0 bend angle where it begins to decrease. The degree of phase separation increases with the increase of mass flux and wall heat flux, decreases with the increase of system pressure. The secondary reverse flow, which drives the coolant to the inner side of the bend, is more dependent on the mass flux.

Current experiment confirmed remarkable differences in heat transfer mechanism over the outer and inner side of the bend. Heat transfer improvement at the outer wall can be attributed to the wet and/or dry collisions of droplets on the wall and the flow acceleration at that region. At the inner wall heat transfer is governed by the degree of phase separation and the development of inward secondary flow appearing in the boundary layer of the cross-section. Dispersed flow heat transfer in bends is significantly enhanced at large mass flux and small wall heat flux. At high reduced pressure, however, the influence of the bend on the flow and heat transfer diminishes greatly.

The purpose of this study is to explore the dispersed heat transfer mechanisms in circular bends. Since the phase re-distribution induced by the bend may influence the heat transfer process to a marked degree, measurements on the void fraction distribution were made by a carefully designed impedance-void-meter. Experimental results on void fraction and heat transfer of the dispersed flow were evaluated in assistance with the droplet dynamics analysis.

2. Experimental Apparatus and Procedure

Experiments on dispersed flow heat transfer in the circular bends were carried out with the refrigerant R12 as modeling fluid. A schematic of the test loop is shown in figure 1.

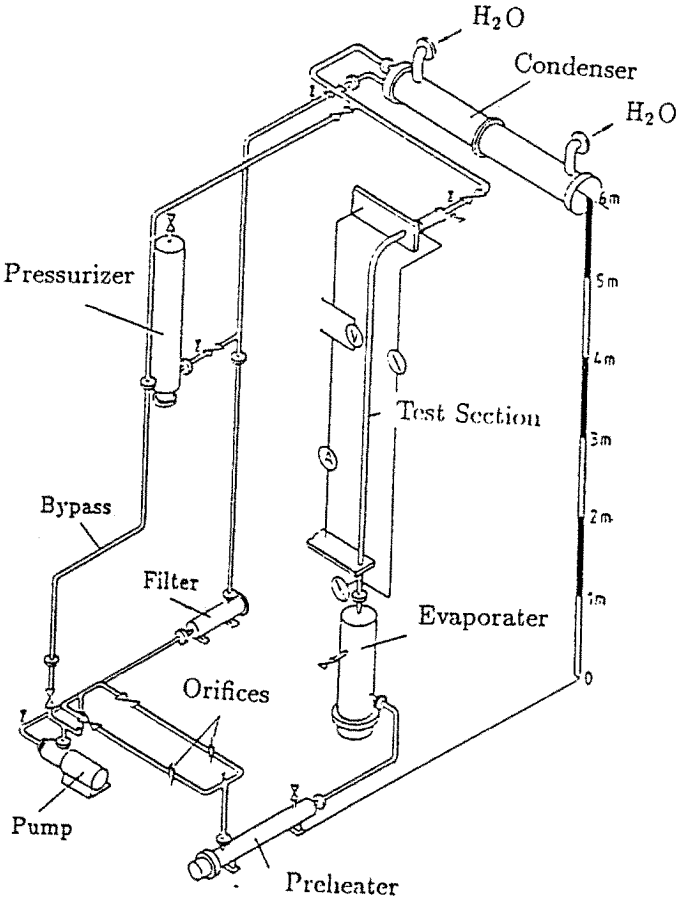

Figure 1. R12 experimental loop

Driven by a centrifugal pump, the refrigerant in the loop first passes through a control valve and an orifice where the mass flux is adjusted and measured. Then it enters into a preheater and an evaporator in which it is heated to a sufficiently high vapor quality before it comes into the test section shown in figure 2. Dryout is regulated to occur in the vertical part of the test section where dispersed two-phase flow starts. After a developing length of 2.5 m, the flow enters into a circular bend where measurements are performed. The two-phase mixture is then condensed in a water-cooled condenser, passes through a filter and flows back to the pump inlet. The system pressure is adjusted by an electrically heated pressurizer installed in the loop.

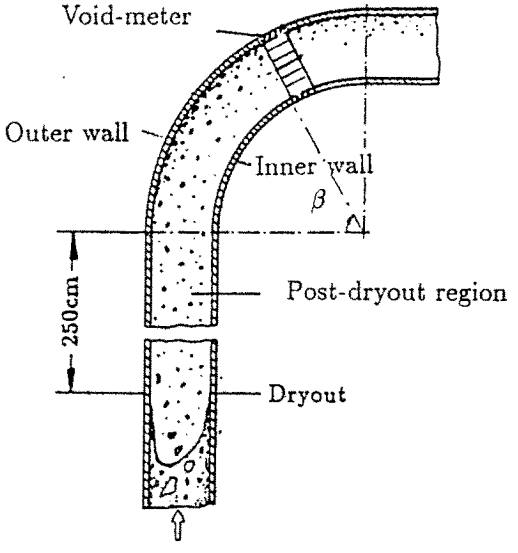

Figure 2. Test section

The test section consists of a vertical straight tube and a 90^0 circular bend heated by direct current. The tube inner diameter is 28.5 mm, and bend radii are 400 mm and 600 mm respectively. 60 chromel-alumel thermocouples, 0.5 mm in diameter, are installed on the outer wall of the test tube. The inner wall temperatures are obtained using the heat conduction equation.

An impedance void meter is installed at 15^0, 30^0, 60^0 angular positions of the bend with radius of 400 mm, and 45^0, 90^0 of the bend with radius 600 mm to measure the local void distribution in five regions of the cross-section and in axial direction. Figure 3 shows a schematic of the void-meter. It consists of thin concentric tubes which are wired to constitute five separate capacitors supplied with a high frequency voltage. On the basis

of different dielectric constants of vapor and liquid , the void fraction in each part of the cross section can be evaluated according to the Maxwell equation for dispersed droplet flow [6]:

$$\alpha = 1 - \frac{1-\epsilon}{\epsilon + 2\epsilon_g} \frac{\epsilon_l + 2\epsilon_g}{\epsilon_l - \epsilon_g} \tag{1}$$

where $\epsilon, \epsilon_g, \epsilon_l$ mean the dielectric constants for two-phase, pure vapor phase and liquid phase respectively, and α means void fraction.

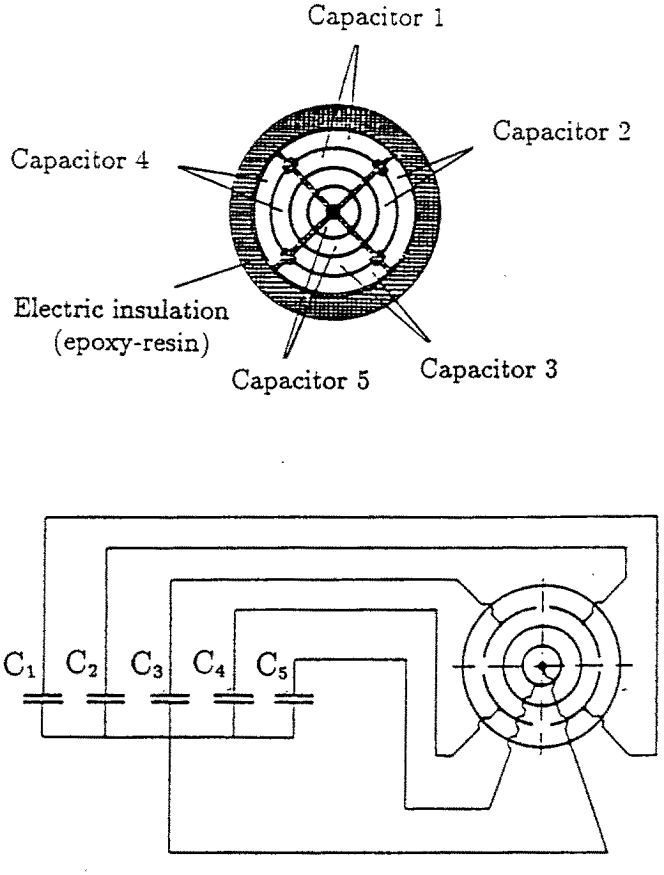

Figure 2. Impedance void meter

In order to minimize the possible condensation during the measurement of droplet distribution, an additional heating element is installed on the void-meter and the down-stream section. The whole experiment is monitored, controlled and recorded with the aid of an HP-1000 computer system.

3. Results and Discussions

Experiments on void fraction and heat transfer of dispersed two-phase flow in vertical circular bends were carried out systematically at various mass fluxes 400, 680, 1240, 2000 kg/m^2s, critical pressure ratios 0.23, 0.46, 0.7, wall heat fluxes 20, 30, 40, 50, 60, 70 kw/m^2, inlet equilibrium qualities 0.45 - 1.15, and bend radius ratios 28 and 42. Void fraction profiles were measured in each of the two 90^0 bends: at $15^0, 30^0, 60^0$ bend angles with radius of 400 mm, and $45^0, 90^0$ bend angles with radius of 600 mm. Results and discussions are presented as follows.

3.1 Analysis of droplet trajectory

At high vapor quality, the void fraction of dispersed flow in the post-dryout region is usually very large. The explanation of heat transfer behavior of the flow in this case is closely associated with the phase distribution, or in a more basic sense, the droplet trajectory characters.

Particle trajectories in turbulent flow fields have been treated by a lot of researchers. They are shown to be mostly determined by the nature of the particle and the effects of the turbulence of the flowing fluid [7]. Due to lack of information concerning the turbulent flow field in short bends, only a simplified calculation is made here aiming at the investigation of the separation effects induced by the centrifugal force and the gravity.

In the present analysis of droplet trajectory, a convenient approach, namely the Lagrangian method is employed, in which individual droplet is tracked through its equation of motion. For simplicity we assumed that the pressure gradient force, virtual mass, Basset history integral and droplet interaction forces are neglected. Evaporation of droplet is not taken into account either.

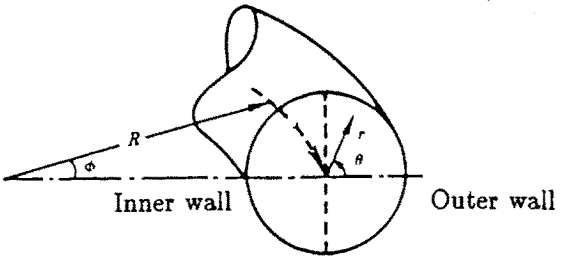

Figure 4. Sketch of coordinate system

Under a toroidal coordinate system (r, θ, ϕ) shown in figure 4, the balance equation for single droplet motion in bends can be expressed as

$$m_d \frac{d\,(v_{d,i}\,\vec{e}_i)}{d\,t} = \sum_j \vec{F}_{j,i}\vec{e}_i \tag{2}$$

where m_d is the mass of the droplet, $\vec{e}_i$ is the unit vector of ith coordinate, $v_{d,i}$ is the droplet velocity in i direction, $F_{j,i}$ is the external force acting on the droplet in direction of i, and j represents different forces including drag force, gravity and buoyancy.

By noting the derivatives of the unit coordinate vector $\vec{e}_i$ with respect to the time t,

$$\frac{d\,\vec{e}_r}{d\,t} = \frac{v_{d,\theta}}{r}\vec{e}_\theta + \frac{v_{d,\phi}cos\theta}{R + rcos\theta}\vec{e}_\phi \tag{3}$$

$$\frac{d\,\vec{e}_\theta}{d\,t} = -\frac{v_{d,\theta}}{r}\vec{e}_r - \frac{v_{d,\phi}sin\theta}{R + rcos\theta}\vec{e}_\phi \tag{4}$$

$$\frac{d\,\vec{e}_\phi}{d\,t} = -\frac{v_{d,\phi}cos\theta}{R + rcos\theta}\vec{e}_r + \frac{v_{d,\phi}sin\theta}{R + rcos\theta}\vec{e}_\theta \tag{5}$$

the equation (2) can be rewritten into three balance equations in the directions of three coordinates:

$$\frac{d\,v_{d,r}}{d\,t} = \frac{v_{d,\theta}^2}{r} + \frac{v_{d,\phi}^2 cos\theta}{R + rcos\theta} + \frac{3}{4}\frac{C_D}{d}\frac{\rho_g}{\rho_l}(v_{g,r} - v_{d,r}) \mid \vec{v}_g - \vec{v}_d \mid - \left(1 - \frac{\rho_g}{\rho_l}\right) g\ cos\theta\ sin\phi \tag{6}$$

$$\frac{d\,v_{d,\theta}}{d\,t} = -\frac{v_{d,r}v_{d,\theta}}{r} - \frac{v_{d,\phi}^2 sin\theta}{R + rcos\theta} + \frac{3}{4}\frac{C_D}{d}\frac{\rho_g}{\rho_l}(v_{g,\theta} - v_{d,\theta}) \mid \vec{v}_g - \vec{v}_d \mid + \left(1 - \frac{\rho_g}{\rho_l}\right) g\ sin\theta\ sin\phi \tag{7}$$

$$\frac{d\,v_{d,\phi}}{d\,t} = -\frac{v_{d,r}v_{d,\phi}cos\theta}{R + rcos\theta} + \frac{v_{d,\theta}v_{d,\phi}sin\theta}{R + rcos\theta} + \frac{3}{4}\frac{C_D}{d}\frac{\rho_g}{\rho_l}(v_{g,\phi} - v_{d,\phi}) \mid \vec{v}_g - \vec{v}_d \mid - \left(1 - \frac{\rho_g}{\rho_l}\right) g\ cos\phi \tag{8}$$

In the above equations, the terms $v_{d,\phi}^2 cos\theta/(R + rcos\theta)$, $v_{d,\phi}^2 sin\theta/(R + rcos\theta)$, are usually referred to as the centrifugal accelerations. The last two terms on the right side of the equations represent the accelerations initiated by the viscous drag, and the combined action of gravity and buoyancy. The parameter C_D is the drag coefficient suggested by James *et al* [8] as $C_D = 0.44 + 24/Re_p$.

Assuming a uniform vapor velocity, and a slip ratio of one at the bend inlet, the above equations can be calculated by using fourth-order Runge-Kutta method. Figure 5 shows some parametric influences on the first impact angle of the droplet on the bend wall (β_I) and the impact velocity normal to the pipe surface $(v_{d,n})$. The velocity $v_{d,n}$ equals to $v_{d,r}\mid_{r=a}$, here a means the tube radius. The Droplet is assumed to enter the bend at the center of the inlet cross-section. Figure 6 shows a typical droplet motion in the circular bend under the most ideal case of elastic impact on the wall.

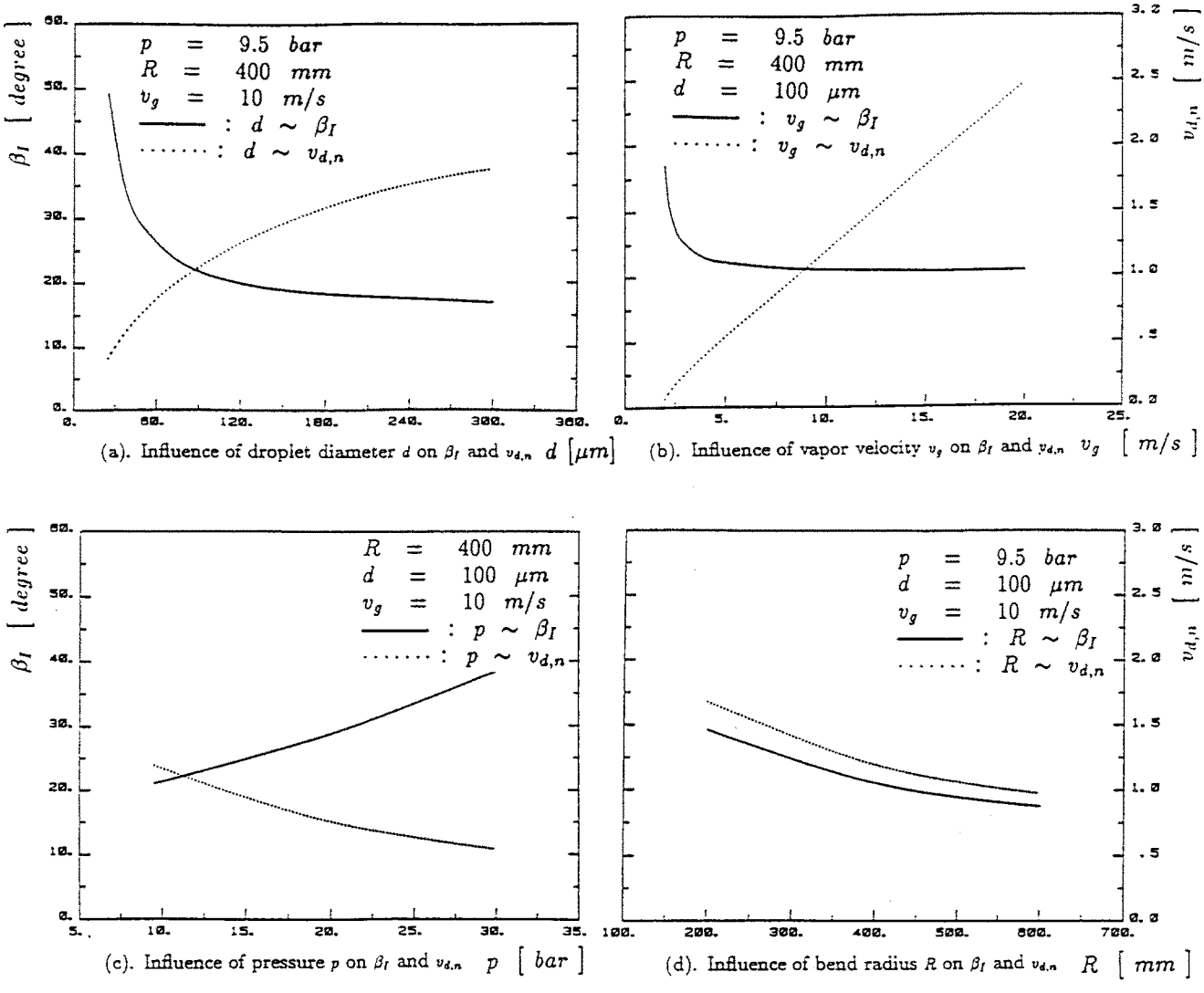

Figure 5. Parametric influences on β_I and $v_{r,n}$

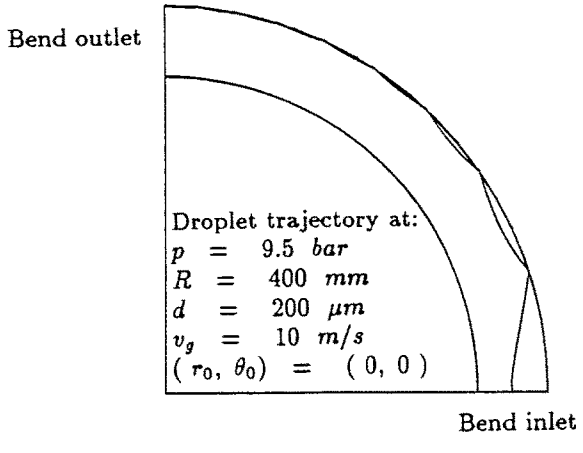

Figure 6. Calculated droplet trajectory

It is shown from the results of simple calculations that the migration of droplets in the bend is determined by the relative importance of the centrifugal force, viscous drag, gravity and buoyancy. For a wide range of flow conditions in the post-dryout region, droplets in the dispersed flow tend to stay near the outer wall region of the bend as shown in figure 6. This means that the outward centrifugal force dominates the droplet motion in the cross-section. As illustrated in figure 5, increasing the droplet diameter, the inlet velocity, and the liquid-to-vapor density ratio leads to an earlier droplet impact on the wall. On the other hand the droplet impact velocity is increased by increasing the droplet dimension, the inlet velocity, and by decreasing the system pressure and bend radius. It should be noted that the normal impact velocity is at least one order of magnitude larger than that in vertical channels as proposed by Liu & Ilori [9]. Hence most droplets can be no longer kept out of the boundary layer, and droplet impact on the outer wall may significantly contribute to the dispersed flow heat transfer in bends.

3.2 Measurement of droplet distributions

Void distribution characters

Under the current experimental ranges, local void concentration measured in five regions of the cross-section and at different axial locations reveals outstanding features in the vertical bends. Figure 7 shows a typical result about void distribution in the bends.

It can be seen from figure 7 that the dispersed flow exhibits a distinct non-symmetric character. The local droplet concentration (*i.e.* one minus void fraction) always keeps its hightest value in the outer wall region of the bend. The phase separation takes place quite early in the downstream of the bend inlet, then develops further along the axial direction. Such development can last to the 60^0 bend angle in the bend with radius of 400 mm. Results with the bend of 600 mm radius indicate that near the bend outlet, the distortion of phase distribution is improved to a certain degree.

As expected from the previous analysis, the droplet motion in the bend is mainly governed by the centrifugal force which drives the droplet moving towards the outer side of the bend. To a spectrum of droplets with different dimensions in dispersed flow, the degree of outward migration is different as shown in figure 5(a). Large droplets deviate more seriously from the vapor stream and impact the outer wall at small bend angles, in present case, as early as 15^0. This results a large increase of droplet concentration at that region. The phase separation can continue as the smaller droplets reaching the outer wall region in the later part of the bend. With the development of the secondary flow, however,

some of the droplets can be driven along the circumferential boundary layer to the inner wall. The phase separation thus decreases at large bend angle.

Parametric influences on void distribution

Experimental evidence indicates that for dispersed flow in bends the void distribution depends strongly on the mass flux and the system pressure.

Figures 8 and 9 show the influence of the mass flux. It can be seen that increasing the mass flux leads to a more pronounced phase separation. This can be explained as follows. Large mass flux is usually associated with high vapor velocity. As stated above, the increase of vapor velocity brings about larger droplet deposition rate. Hence the droplets at large mass flux have greater kinetic energy in contact with the outer wall resulting in a better heat transfer at that region. The decrease of vapor superheating at the outer wall region makes it more easier for the following droplets, even with smaller energy, to accumulate there. The formation of a liquid film on the outer wall is sometimes possible if the droplet deposition flux is sufficiently large and the wall heat flux is not high. Besides, as the primary flow increases, so does the secondary reverse flow which can transport more droplets along the circumference of the cross section to the inner wall. Due to the high droplet evaporation rate and the action of secondary flow, the droplet concentration in the outer wall region at large bend angle decreases appreciably at large mass flow rate.

System pressure also plays an important role upon the droplet distributions. Figure 10 together with figure 8(a) shows a comparison of this influence. Under low pressure, a developed pattern of droplet concentration is formed early in the bend angles from 15^0 to 30^0. The droplet concentration in the outer wall region is normally much larger than the one in other parts of the cross-section. However, when the pressure becomes higher, the structure of dispersed flow changes gradually along the bend. A significant circumferential gradient of local droplet concentration can be observed with its maximum in the outer wall region and the minimum in the inner wall region of the cross-section. These phenomena can be explained again by the previous analysis of droplet motion in bends. When the system pressure, or the vapor-to-liquid density ratio increases, the droplet dimension and the mixture inlet velocity decrease in this experimental system [10]. Therefore the liquid droplets can be deflected more easily and behave similar like the elements of the vapor stream. The reduction of void fraction in the inner wall region at large bend angle is presumably attributed to the reverse transportation of droplets by the secondary flow.

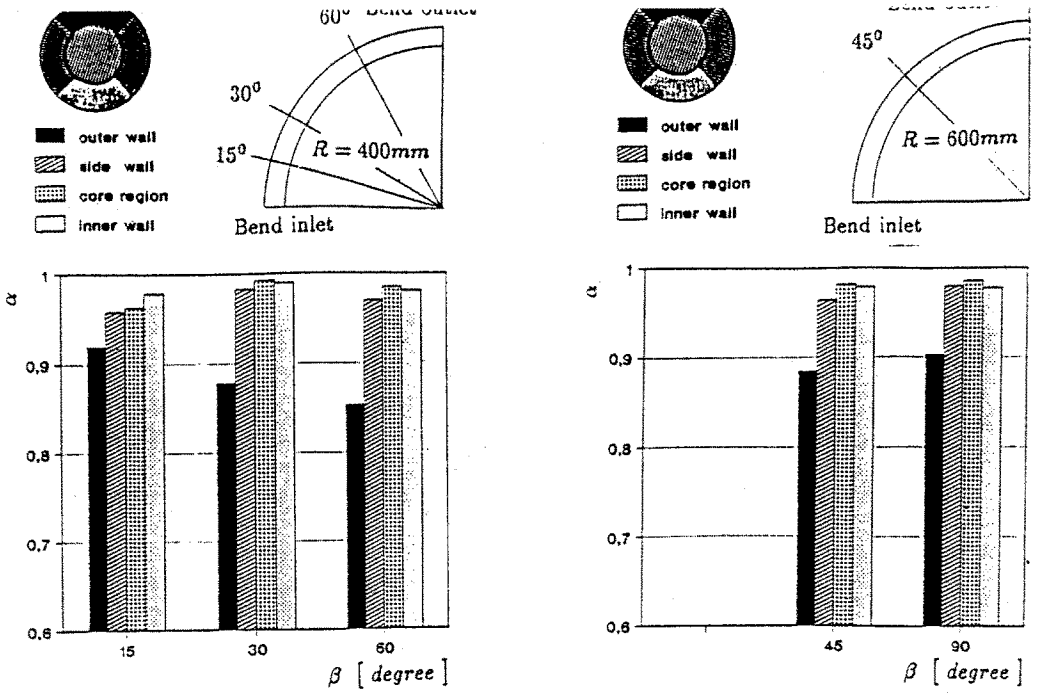

(a). Measurement with R = 400 mm (b). Measurement with R = 600 mm

Figure 7. Void fraction distributions in bends at:
P = 9.5 bar, G = 680 kg/m²s, q''_w = 50 kw/m²

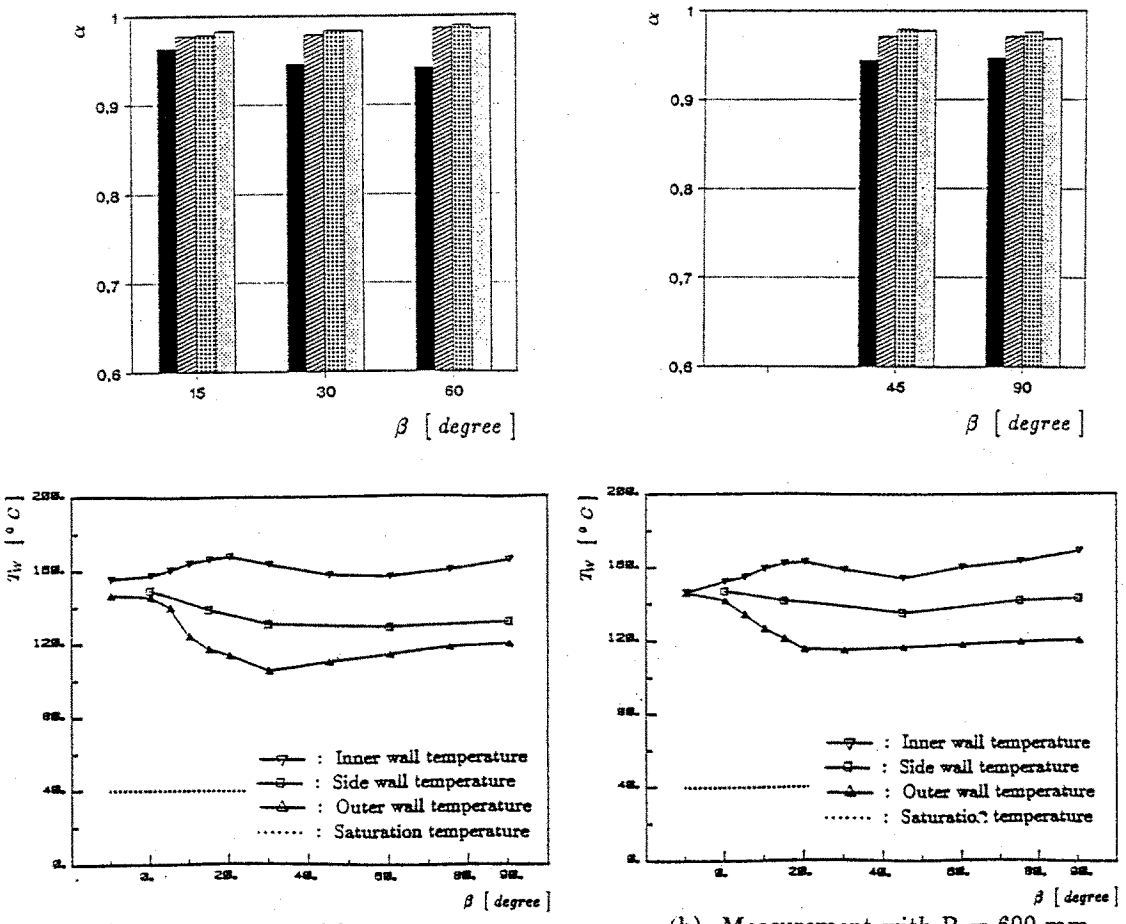

(a). Measurement with R = 400 mm (b). Measurement with R = 600 mm

Figure 8. Void fraction and temperature distributions in bends at:
P = 9.5 bar, G = 400 kg/m²s, q''_w = 30 kw/m²

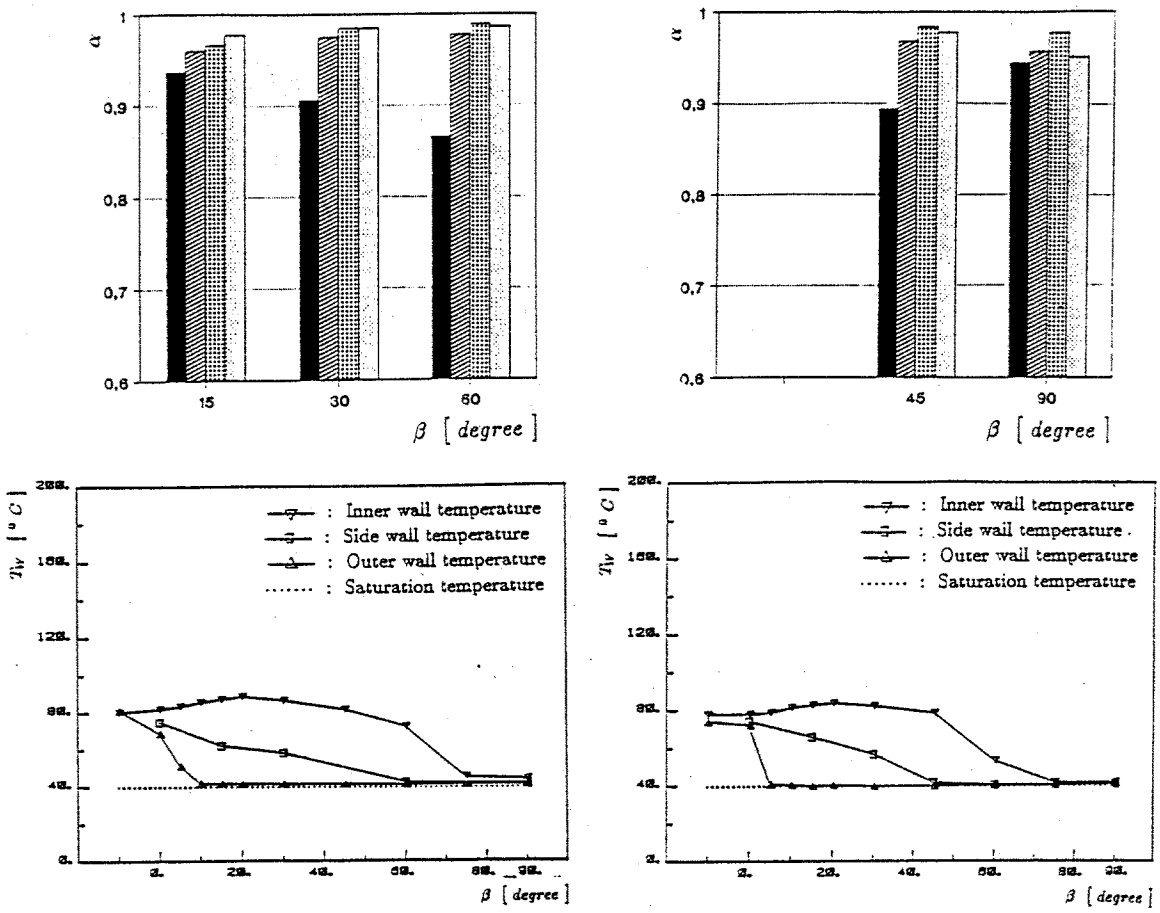

(a). Measurement with R = 400 mm (b). Measurement with R = 600 mm

Figure 9. Void fraction and temperature distributions in bends at:
P = 9.5 bar, G = 1200 kg/m²s, q''_w = 30 kw/m²

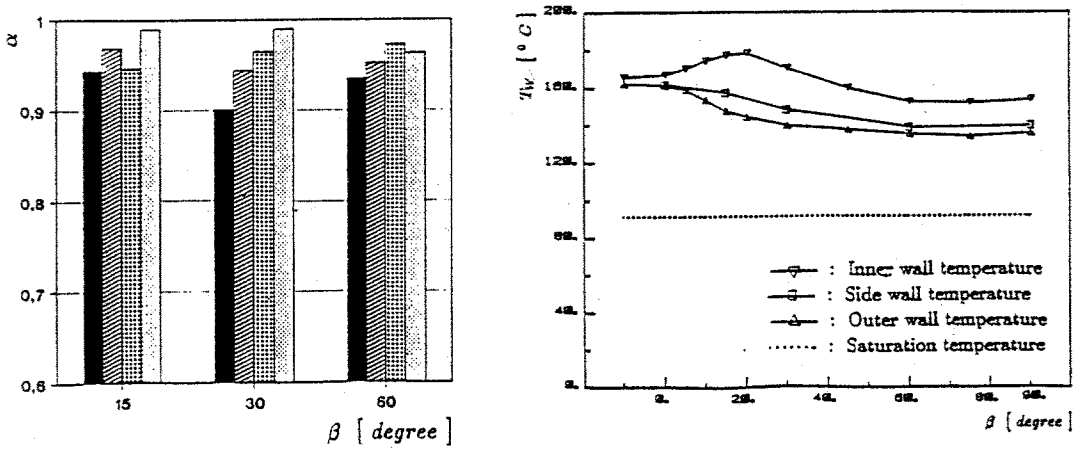

Figure 10. Void fraction and temperature distributions in bend with R = 400 mm at:
P = 28.5 bar, G = 400 kg/m²s, q''_w = 30 kw/m²

3.3 Analysis of the heat transfer mechanisms

Test results on the void fraction and wall temperature distributions indicate that heat transfer of the dispersed flow in bends is influenced dramatically in two ways: strong outward migration of droplets; and improved vapor convection due to the droplets evaporation and onset of the secondary flow. From measurements, two different heat transfer patterns can be found, namely non-rewetting heat transfer and rewetting heat transfer.

Heat transfer in rewetting conditions

As shown in figure 9, rewetting of droplets on the wall is one of the characteristics of the dispersed flow heat transfer in the bend. This phenomenon is usually associated with a combination of low wall heat flux, intermediate to large mass flux and low pressure. Previous studies on droplets-wall heat transfer [11] [12], indicated that such process is primarily dependent upon the impinging droplet Weber number ($\varrho_l v_{d,n}^2 d/\sigma$) and the wall superheating ($T_w - T_{sat}$). At large mass flux and low pressure, the local droplet concentration in the outer wall region is relatively high. This implies that there exists a high droplet deposition flux. Once the droplets reach the outer wall, they may deform there as flattened bodies provided the wall heat flux is low. These discrete bodies are easily linked together by the later impinging droplets thus forming a thin liquid film. If the film is maintained, the rewetting heat transfer starts at the outer wall as revealed by wall temperature. When the deposition rate is high enough, the liquid film can be stretched into the inner part of the bend by the pressure force after an axial distance. The wall temperature measurements in figure 9 show a gradual occurrence of rewetting from the outer wall to the side wall, and finally to the inner wall. The circumferential inward motion of liquid film is also qualitatively confirmed by the local droplet distributions: at large bend angle, droplet concentrations decrease gradually from the outer wall to the inner wall regions while the concentration in the core region has the lowest value in the cross-section. It is therefore certain from the experiments that the heat transfer improvement in the outer wall region is attributed to the wet collisions of the droplets as well as the flow acceleration at that region. The heat transfer in the inner wall is more dependent upon the degree of phase separation. It is deteriorated at first due to the liquid deficiency and deceleration of the vapor flow, then improved due to the coolant reversal and even the inward development of the liquid film.

Heat transfer in non – rewetting conditions

At low mass flux, high heat flux and in most cases at high system pressure, the non-rewetting heat transfer in the bend is prevailing. Figures 8 and 10 show measurements in non-rewetting conditions.

Conditions of non-rewetting heat transfer coincide with high void fraction. In the outer wall region, however, there still exists a relatively large droplet concentration compared with the other parts of the cross section although the pipe wall is highly superheated. From the outer wall temperature distributions one can find an improvement of heat transfer in the early part of the bend, then a gradual deteroriation in the later part of the bend. On the other hand, heat transfer at the inner wall is weekened at first then improved a little, and again weekened at large bend angle.

The non-rewetting heat transfer behavior can be well explained by analysing the vapor flow structure and single droplet behavior because of the diluted character of the dispersed flow.

Due to the high wall superheating, droplets are always kept out of the boundary layer by the thermal reaction forces. Heat transfer by the droplet dry collisions is much less effective than that by the droplet wet collisions. Hence the mechanism of vapor convection becomes very important. Vapor convective heat transfer of the dipersed flow is composed of two contributions: the convection due to the bulk vapor flow and the local turbulence convection induced by the presence of droplets. As pointed out above, the bulk flow accelerates in the outer wall region and decelerates in the inner wall region. The droplet evaporation in the outer wall region may enhance this acceleration. Moreover, the local turbulence convection may also increase due to the addition of droplets in that region. Both of these two effects can result in an improvement of the heat transfer. As a certain portion of droplets evaporate or flow away, the heat transfer may be deteriorated at the outer wall region at large bend angle. For the inner wall region, since the void fraction is very high, the heat transfer depends mainly on the convection of the bulk vapor flow. In this case, the deterioration of inner wall heat transfer due to the flow deceleration can be improved by the development of the secondary flow to a certain degree. However, this improvement may be greatly reduced if heat transfer is already deteriorated in the outer wall region.

4. Conclusions

1). Measurements of local droplet distributions in dispersed flow in bends reveal a distinct non-symmetric character with the maximum value shifted to the outer wall region.

2). Phase separation can occur quite early in the vertical bends. This process is influenced by mass flux, the system pressure, and the heat flux with a pronounced dependence on the mass flux.

3). Dispersed flow heat transfer is greatly improved in the outer wall region due to the strong outward migrations and collisions of droplets, and the flow acceleration. The inner wall heat transfer is governed by the degree of phase separation and the vapor convection.

References

[1] F. Mayinger:
Strömung und Wärmeübergang in Gas-Flüssigkeits-Gemischen
Springer-Verlag, 1982

[2] F. Varone Jr., W.M. Rohsenow:
Post-dryout heat transfer prediction
Nucl. Engn. & Design, Vol.95, 315, 1986

[3] Y. Mori, W. Nakayama:
Study on forced convective heat transfer in curved pipes
Int. J. Heat Mass Transfer, Vol.10, 57, 1988

[4] M. Rowe
Measurements and computations of flow in pipe bends
J. Fluid Mech. Vol.43, part 4, 771, 1970

[5] G. Lautenschlager
Wämeübergang in Krümmern bei Sprühkühlung
Dr. Thesis, T.U. München, 1988

[6] L. Maxwell
A treatise on electricity and magnetism
Oxford University Press, Oxford, 1873

[7] A. Berlemont, et al
Particle Lagrangian simulation in turbulent flows
Int. J. Multiphase Flow, Vol.16, No.1, 19, 1980

[8] P.W James, et al
Droplet motion in two-phase flow
UKAEA Report AERE-R9711, 1980

[9] B.Y.H. Liu, T.A. Ilori
Aerosol deposition in turbulent pipe flow
Environmental Sci. & Tech. Vol.8, 351, 1974

[10] G. Lautenschlager, F. Mayinger
Post-dryout heat transfer in curved tubes
European two-phase flow meeting, München, 1986

[11] E.N. Ganic, W.M. Rohsenow
Dispersed flow heat transfer
Int. J. Heat Mass Transfer Vol.20, 855, 1977

[12] K.J. Choi, S.C. Yao
Mechanisms of film boiling heat transfer of normally impacting spray
Int. J. Heat Mass Transfer Vol.30, 311, 1987